# Relative sizes of $^{40,48}$Ca from the scattering of 79 MeV $\alpha$ particles

G. M. Lerner,* J. C. Hiebert, and L. L. Rutledge, Jr.†
*Cyclotron Institute‡ and Physics Department, Texas A&M University, College Station, Texas 77843*

C. Papanicolas and A. M. Bernstein
*Physics Department and Laboratory for Nuclear Science,§ Massachusetts Institute of Technology, Cambridge, Massachusetts 02139*
(Received 7 October 1974; revised manuscript received 21 April 1975)

The scattering of 79.1 MeV $\alpha$ particles from $^{40,48}$Ca has been measured with high relative accuracy and analyzed with a folding model for the optical potential. The result for $\Delta R$, the difference between the $^{40,48}$Ca rms matter radii, is $\Delta R = 0.05 \pm 0.04$ fm. This result appears smaller than most previous measurements which employed Woods-Saxon potentials or diffraction analyses. Most of the discrepancies are removed when the definition of the matter radius used in each analysis is scrutinized. Combining $\Delta R$ with the results of electromagnetic experiments yields the relative neutron-proton radius difference in $^{48}$Ca; $R_n(48) - R_p(48) = 0.03 \pm 0.08$ fm. These results are compared with Hartree-Fock calculations which tend to produce larger differences. Possible reasons for this discrepancy are discussed.

[NUCLEAR REACTIONS $^{40,48}$Ca$(\alpha,\alpha)$ $E = 79.1$ MeV; measured $\sigma(\theta)$; $\theta = 10$–$45°$, enriched targets. Microscopic optical model analysis; deduced rms matter radii.]

## I. INTRODUCTION

The problem of the relative sizes of the doubly closed shell nuclei $^{40,48}$Ca is of considerable interest. From electron scattering[1] and muonic x-ray studies[2] it was found that the relative rms radii of the charge distributions is $\Delta R_c = R_c(48) - R_c(40) = -0.01$ fm. Since $\Delta R_c$ was interpreted as equal to the difference of the rms proton radii $\Delta R_p = R_p(48) - R_p(40)$, this negative result was surprising since both $^{42}$Ca and $^{44}$Ca have $R_c > R_c(40)$. Recently it has been noted[3] that because of certain relativistic effects and because of the charge form factor of the neutron $\Delta R_c \neq \Delta R_p$ and the value $\Delta R_p = +0.012$ fm was obtained, thereby resolving the $^{48}$Ca anomaly.

It is also of interest to determine the relative neutron or total density rms radii. To do this we have utilized $\alpha$ particle scattering for which the optical potential $U(r_\alpha)$ has been approximately related to the density distribution of nucleons $\rho(r)$ by[4-9]:

$$U(r_\alpha) = (\lambda_r + i\lambda_i) \int \rho(r) V_{\text{eff}}(\vec{r} - \vec{r}_\alpha) d\tau \qquad (1a)$$

or

$$U(r_\alpha) = \left(\lambda_r - i\delta_i \frac{d}{dr_\alpha}\right) \int \rho(r) V_{\text{eff}}(\vec{r} - \vec{r}_\alpha) d\tau , \qquad (1b)$$

where $\lambda_r$ and $\lambda_i$ (or $\delta_i$) are empirical functions of $E_\alpha$ (the $\alpha$ particle energy), $\rho(r)$ is normalized to $A$ nucleons, and $V_{\text{eff}}(\vec{r} - \vec{r}_\alpha)$ is the effective $\alpha$ particle bound nucleon interaction. $V_{\text{eff}}$ has been obtained[6,8] by averaging a nucleon-nucleon interaction[10] which fits the low energy nucleon-nucleon data over the empirical $\alpha$ particle size (as determined by electron scattering). This gives:

$$V_{\text{eff}}(\vec{r} - \vec{r}_\alpha) \cong V_0 \exp\left[-\left(\frac{\vec{r} - \vec{r}_\alpha}{r_0}\right)^2\right], \qquad (2)$$

where $V_0 = 37$ MeV and $r_0 \cong 2.0$ fm.[6,8]

The parameters $\lambda_r$ and $\lambda_i$ (or $\delta_i$) have been determined from $\alpha$ particle scattering from the $T = 0$ nucleus $^{40}$Ca for which $\rho_n(r) \cong \rho_p(r)$ and $\rho_p(r)$ is obtained from electron scattering. Theoretical angular distributions obtained using Eqs. (1a) and (1b) are compared to the measured angular distribution in Fig. 1(a). Values obtained for the parameters were $\lambda_r = 1.018$, $\lambda_i = 0.473$ for Eq. (1a) and $\lambda_r = 0.978$, $\delta_i = 0.383$ for Eq. (1b). It has been previously shown[11] that $\lambda_r$ ($\lambda_i$) decreases (increases) approximately linearly with increasing $E_\alpha$.

For each $E_\alpha$, the parameters $\lambda_r$ and $\lambda_i$ ($\delta_i$) are taken as fixed. Utilizing theoretical values for the matter density one can predict the elastic scattering of $\alpha$ particles without any adjustable parameters. An example of this is given in Fig. 1(b) for $^{40}$Ca using the Hartree-Fock (HF) calculations of Negele[12] and Miller and Green.[13] It can be seen that these HF calculations are in good agreement with the data. This is not surprising since Miller and Green[13] chose their parameters to give the correct rms radius for $^{40}$Ca and Negele's calculations[12] are in good agreement with electron scattering.

It is important to realize that it is because of the composite nature of the $\alpha$ particle that the scattering is characterized by strong absorption.

Consequently only the potential in the surface region is important for the forward diffraction region of scattering, and the data should be insensitive to the details of $V_{\text{eff}}$. These considerations are presented quantitatively in Sec. IIID in a discussion of the systematic errors and are considered in detail in Ref. 6.

The relationship between $U(r_\alpha)$ and $\rho(r)$ [Eq. (1)] has been tested by successfully predicting[5] $\alpha$ particle scattering from the $N=Z$ nuclei $^{28}$Si and $^{16}$O. It has also been shown that ±10% deviations in $r_0$,

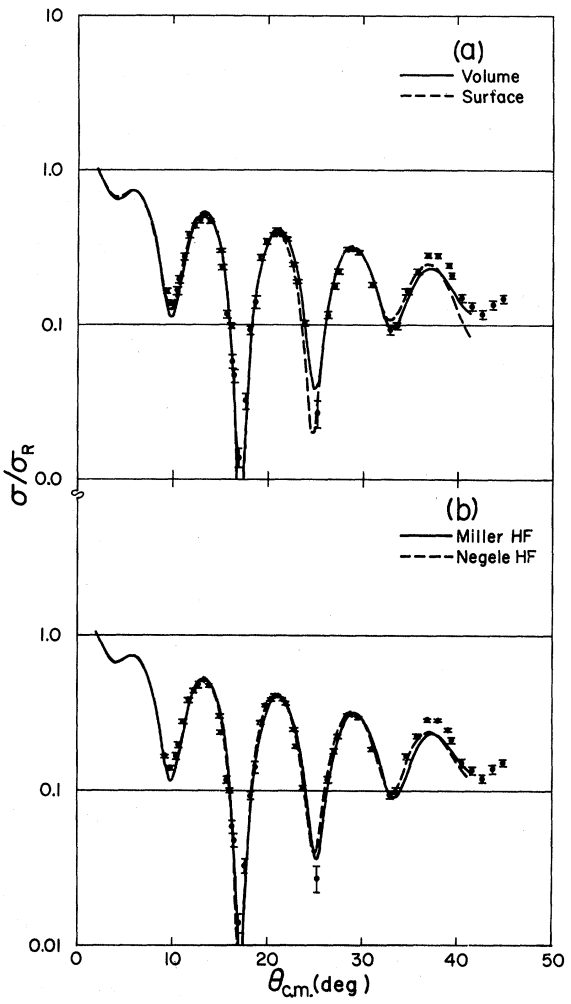


FIG. 1. Differential cross sections for the elastic scattering of 79.1 MeV $\alpha$ particles from $^{40}$Ca plotted as the ratio to Rutherford scattering. In part (a) the curves are obtained from best fits to the data. The solid curve uses Eq. (1a) and the dashed curve uses Eq. (1b). Part (b) shows the predicted angular distributions using the Hartree-Fock densities of Negele (Ref. 12) and Miller and Green (Ref. 13). In all subsequent figures showing cross sections the reaction will be the elastic scattering of 79.1 MeV $\alpha$ particles unless otherwise stated.

the range of $V_{\text{eff}}$, do not alter the predictions using Eq. (1) provided that the values of $\lambda_r$ and $\lambda_i$ (or $\delta_i$) are readjusted.[6] Using these results, matter distributions in the surface region for many $N \neq Z$ nuclei have been obtained[5-7] from elastic scattering data. Once $\rho(r)$ is known, the neutron distribution $\rho_n(r) = \rho(r) - \rho_p(r)$ is obtained by subtracting the empirical proton distributions found in electron scattering experiments.

It has been estimated that nuclear sizes can be measured to an accuracy of approximately 0.1 fm by $\alpha$ particle scattering.[6] Furthermore it is possible that the relative sizes of a series of isotopes (or isotones) can be measured with even higher relative accuracy. Because the size difference of a pair of isotopes is small one must make careful relative measurements (see Sec. II) and analyses of the differences (Sec. III).

The relative sizes of $^{40,48}$Ca have been previously studied using protons,[14,15] $\alpha$ particles,[7,16,17] and $^{16}$O ions.[18] Several authors determined empirical optical potentials, defined a radius $R_V$, of this potential or a strong absorption (diffraction) radius[15-18] and obtained $\Delta R_V = R_V(48) - R_V(40)$. Some confusion has arisen because of the assumption[15,17] that $\Delta R_V = \Delta R$, the difference in the rms matter radii of $^{40,48}$Ca. This assumption is incorrect due to the different normalizations of the density distributions for the two nuclei [see Eq. (4)]. Because of this difference, even if $\Delta R = 0$, one would have $\Delta R_V \cong 0.15$ fm. This is discussed in Sec. III and a comparison with the previous experiments is presented in Sec. IV.

Several methods have been proposed to measure neutron or total density distributions.[19,20] Of these only the method of Coulomb energy differences[19] has been applied to $^{40,48}$Ca. A comparison with this method will be presented in Sec. IV.

## II. DATA ACQUISITION

The differential cross sections of elastically scattered 79.1 ± 0.1 MeV $\alpha$ particles from $^{40}$Ca and $^{48}$Ca have been measured at the Texas A&M University Cyclotron Institute. The targets were self-supporting foils (0.24 mg/cm$^2$ natural CaO and 0.94 mg/cm$^2$ CaO enriched to 98% in $^{48}$Ca). The scattered $\alpha$ particles were detected with two 3 mm Si(Li) detectors separated by a 5.5° angle in a single rotatable mount. Angular acceptance was 0.3° for each detector and energy resolution was about 150 keV [full width at half-maximum (FWHM)]. Absolute cross sections were obtained by reducing the beam energy to 24.2 MeV and measuring differential cross sections between 5 and 15° (lab). Comparing these data which extend into the Rutherford scattering region to optical

model predictions yielded absolute cross sections for the 79 MeV data believed accurate to 5%. In addition, scattering from the natural $^{40}$CaO target was compared with that from a weighed Ca metal standard. Relative cross section accuracy was limited to approximately 1% by background subtraction errors and to 5% near deep minima in the angular distributions due to statistics. Error bars in the figures include statistical, background subtraction, and, where applicable, relative $^{40}$Ca to $^{48}$Ca normalization errors.

Data were always taken on the two calcium targets before changing the laboratory angle. This procedure insures that the relative angular accuracy for the $^{40}$Ca and $^{48}$Ca measurements is very high. Monitor detectors above the scattering plane on either side of the beam were used to determine drifts in beam position during the course of a bombardment. Using these monitor data, the angular error between $^{40,48}$Ca measurements was determined to be less than 0.1°. The absolute laboratory angles and the Faraday cup efficiency were determined by measuring small angle scattering on both sides of the beam using a gold target of known thickness.

## III. ANALYSIS OF RESULTS

### A. Diffraction analysis

Since the radii of the Ca isotopes do not differ by very much it is advantageous to utilize difference methods to analyze the data rather than analyze each isotope independently. The first method of analyzing the data is based on the diffraction model[8,21] which predicts than an increase of radius of $^{48}$Ca relative to $^{40}$Ca would be manifested by the diffraction pattern of the $^{48}$Ca angular distribution shifting to smaller angles relative to $^{40}$Ca. As is indicated in Fig. 2, we measured $\Delta\theta_{1/2}$, the angular difference between the points at which each cross section is half of its nearest maximum value, for the corresponding diffraction maxima.

Theoretical curves using the potential of Eq. (1a) to calculate $\sigma(\theta)$ were obtained for a series of assumed $^{48}$Ca densities of varying radii and are plotted in Fig. 3(a). Since $\alpha$ particles interact in the surface region[6] it is sufficient to characterize $\rho(r)$ by the Fermi form

$$\rho(r)=\rho_0\left[1+\exp\left(\frac{r-c}{a}\right)\right]^{-1}, \tag{3}$$

where $\rho_0$ is determined from the normalization condition:

$$\int \rho(r)d\tau = A \tag{4}$$

nucleons. For $^{40}$Ca the parameters were chosen to give a close match to the empirical proton distribution, i.e., the empirical charge distribution[22] with the finite size of the proton unfolded. Calculations for $^{48}$Ca were performed by varying the parameters $\Delta c = c(48) - c(40)$ and $\Delta a = a(48) - a(40)$.

It has been shown[6] that in the $A = 40$–$48$ mass region it is only the rms radius $R$ of $\rho(r)$ and not the individual parameters $c$ and $a$ to which $\sigma(\theta)$ is sensitive in the diffraction region. This was confirmed in the present study by adjusting $\Delta c$ and $\Delta a$ and observing that the results depend only on $\Delta R$. The results presented in Fig. 3(a) indicate a monotonic change in $\sigma_{48}(\theta)$ with increasing $\Delta R$. It is important to note that the curves for $^{40,48}$Ca are quite different even for $\Delta R = 0$. It can be shown that this difference is not a center of mass effect but occurs because of the normalization of $\rho(r)$ [Eq. (4)]. Figure 3(b) shows $\rho(r)$ for $^{40,48}$Ca in the region of the nuclear surface with $\Delta R = \Delta c = \Delta a = 0$. The main contribution to elastic $\alpha$ particle scattering comes from the region where the nuclear matter density is 5–15% of the central density.[6] The most sensitive region is near the radius $\bar{r}$, defined by the condition[6] $\rho(r=\bar{r}) \cong 0.017$ nucleons/fm$^3$ (see Fig. 14 and the discussion in Sec. III D). Even with $\Delta R = 0$, the construction in Fig. 3(b) shows that $\Delta\bar{r} = \bar{r}(48) - \bar{r}(40) = 0.11$ fm. This consequence of the normalization of the nuclear matter density Eq. (4) is quite important in understanding the results of previous analyses of the $^{40,48}$Ca differences (see Sec. IV).

To obtain $\Delta R$ from a diffraction analysis successive values of $\Delta\theta_{1/2} = \theta_{1/2}(40) - \theta_{1/2}(48)$ are plotted vs $\theta = \frac{1}{2}[\theta_{1/2}(40) + \theta_{1/2}(48)]$. This is done with the measured angular distributions and with predicted

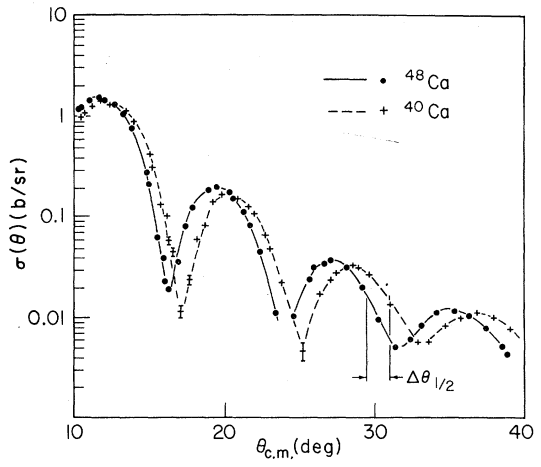


FIG. 2. Scattering cross sections from $^{40,48}$Ca. The lines through the data have no theoretical significance. The construction of $\Delta\theta_{1/2}$ for $\theta \approx 30°$ is illustrated (see text for discussion).

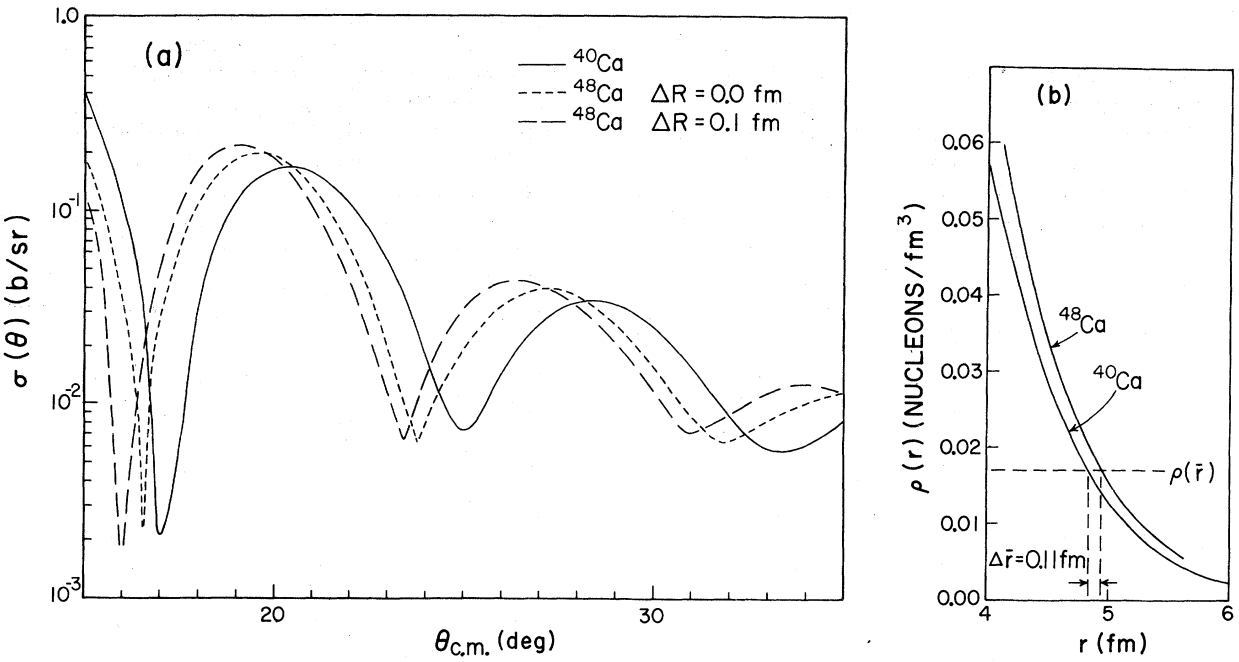


FIG. 3. Part (a): Cross sections for scattering from $^{40,48}$Ca with different assumed values for $\Delta R = R(48) - R(40)$. Part (b) shows $\rho(r)$ for $^{40,48}$Ca in the surface region with the assumption that $\Delta R = 0$. The radius $\bar{r}$ is defined by the condition $\rho(\bar{r}) = 0.017$ nucleons/fm$^3$. The construction of $\Delta\bar{r} = \bar{r}(48) - \bar{r}(40)$ which is 0.11 fm for this case is also shown.

angular distributions. The results are presented in Fig. 4(a) for the present experiment and a similar set in Fig. 4(b) for the 42 MeV data of Fernandez and Blair.[16] It can be seen from a comparison of theory and experiment that $\Delta R = 0.05 \pm 0.04$ fm for both sets of data. The uncertainties quoted here represent only the fitting errors and not any systematic errors in the model employed. The results of the diffraction analysis are presented in Table I.

### B. Isotopic difference function

The diffraction analysis has the advantage that it directly relates the differences in the observed cross sections to $\Delta R$. It does not depend on the measurement of absolute cross sections but only upon the relative angular accuracy which is essentially perfect; however, it does single out a special region of the cross section. A more usual procedure is to weigh each experimental point as the square of its inverse error. To do this we have employed the isotopic difference function $D(\theta)$:

$$D(\theta) = \frac{\sigma_{48}(\theta) - \sigma_{40}(\theta)}{\sigma_{48}(\theta) + \sigma_{40}(\theta)} , \qquad (5)$$

where the differential cross sections are in the center of mass (c.m.) system and the angles are in the laboratory system.

The use of the isotopic difference function has several advantages over the more usual technique of fitting to each isotope separately. In addition to the primary consideration, a possible increased sensitivity to small density differences, $D(\theta)$ is independent of errors in absolute normalization and the relative normalization may be checked by noting that for isotopes $\lim D(\theta) = 0$ as $\theta \to 0$. Fitting high energy $\alpha$ data is often complicated by problems of angular resolution and accuracy near deep minima of the diffraction pattern; the isotopic difference function maps these data points into ±1 with small errors. Thus one avoids the problem of assigning unrealistic weights to data.

TABLE I. Results for $\Delta R = R(48) - R(40)$ where the $R$'s are rms radii. The errors are estimated from fitting the data. See Sec. IIID for estimates of the systematic errors.

| Method | $E_\alpha$ (MeV) | $\Delta R$ (fm) |
|---|---|---|
| Isotopic difference function | 79.1 | 0.02 ± 0.04 |
| Diffraction analysis | 79.1 | 0.05 ± 0.04 |
| Isotopic difference function | 42 | 0.07 ± 0.06 |
| Diffraction analysis | 42 | 0.05 ± 0.04 |
| Average | | 0.05 ± 0.04 |

Figure 5–7 illustrate the relationship between $D(\theta)$ and the density difference. The optical potential was taken to have the form of Eq. (1a) with $V_{\text{eff}}$ given by Eq. (2). For both isotopes a Fermi matter distribution is assumed with $c(40) = 1.2A^{1/3}$ fm and $a(40) = 0.5$ fm. The effect upon $D(\theta)$ of changing only $c(48)$ is shown Fig. 5. Increasing the size of $^{48}$Ca relative to $^{40}$Ca increases the maxima and minima of $D(\theta)$ and shifts the pattern to smaller angles. A similar result is obtained if we set $c(48) = c(40)$ and only adjust the diffuseness for $^{48}$Ca as shown in Fig. 6. The conclusion that $D(\theta)$ is primarily sensitive to the difference in rms radii not to $\Delta c$ or $\Delta a$ is illustrated in Fig. 7. The solid curve was obtained with $\Delta c = 0.2$ fm, $\Delta a = 0$, and $\Delta R = 0.13$ fm whereas the dotted curve corresponds to $\Delta c = 0$, $\Delta a = 0.06$ fm, and $\Delta R = 0.13$ fm. Thus $\Delta R$ is a meaningful parameter in fitting the isotopic difference function.

Figure 8 illustrates the normalization effect for the isotopic difference function (see discussion in Sec. III A). The dashed line corresponds to an identical shape $\rho_{48}(r) = (48/40)\rho_{40}(r)$ for the densities and the agreement with experiment is good. This agreement indicates that $\Delta R$ is small. The effect of the center of mass energy difference on $D(\theta)$ has been calculated by assuming that the optical potentials are the same for $^{40,48}$Ca. This calculation is shown as a solid line in Fig. 8 and the effect is seen to be negligible.

In the discussion of Figs. 5–8 the emphasis was on the qualitative aspects of $D(\theta)$. The following discussion concentrates on fitting $D(\theta)$ to the data. To do this a Fermi form was assumed for the density distribution of $^{48}$Ca. The parameters $c(48)$ and $a(48)$ were then varied to produce a minimum $\chi^2$ where

$$\chi^2[c(48), a(48)] = \frac{1}{N-2} \sum_{i=1}^{N} \left( \frac{D_{\text{theory}}(\theta_i) - D_{\text{exp}}(\theta_i)}{\epsilon_i} \right)^2 , \tag{6}$$

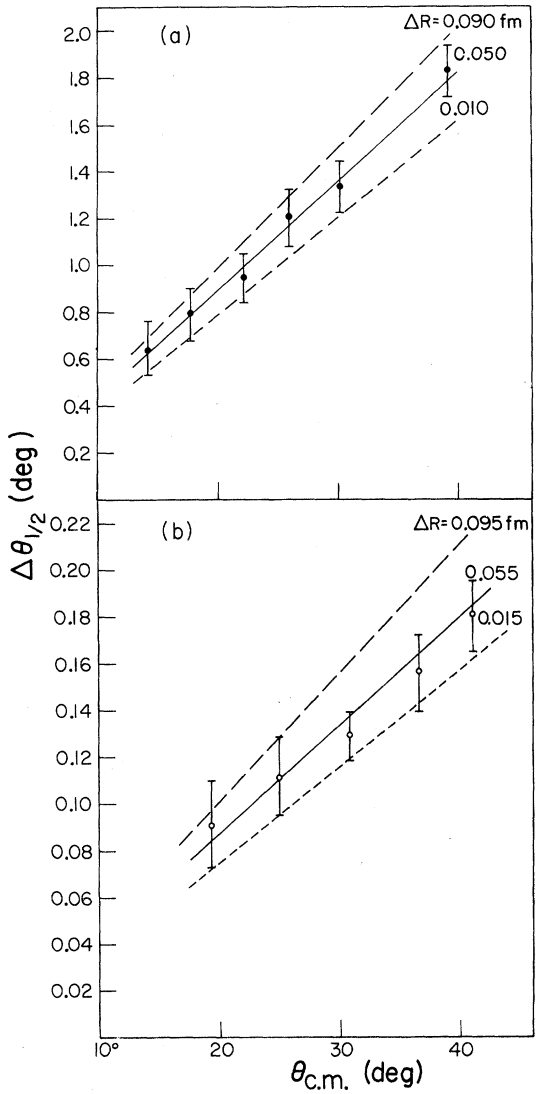


FIG. 4. $\Delta\theta_{1/2}$ versus $\theta$. Experimental points are shown with error bars. The solid line represents the best fit to the data and the dashed lines the error limits. These curves are labeled with their respective $\Delta R$ values in fm. Part (a) contains the 79 MeV results and part (b) is the 42 MeV data of Ref. 16.

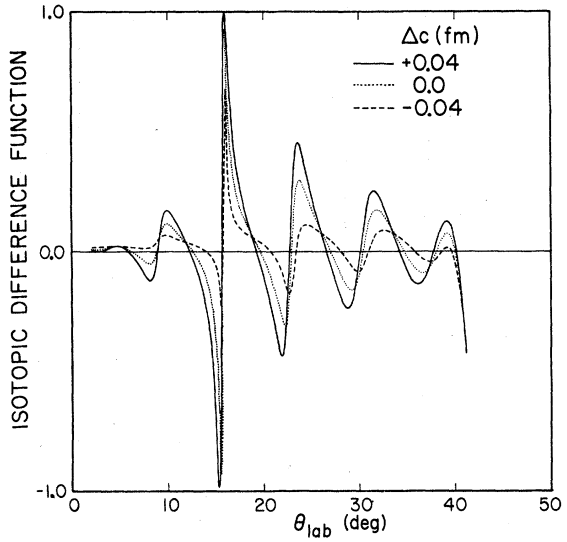


FIG. 5. Isotopic difference function $D(\theta)$ versus $\theta_{\text{lab}}$. The variation of the $D(\theta)$ with $\Delta c = c(48) - c(40)$ is shown. In Figs. 5–9 and 11 $D(\theta)$ is shown for the elastic scattering of 79.1 MeV $\alpha$ particles from $^{40,48}$Ca. Experimental points are shown with error bars and theoretical curves are labeled.

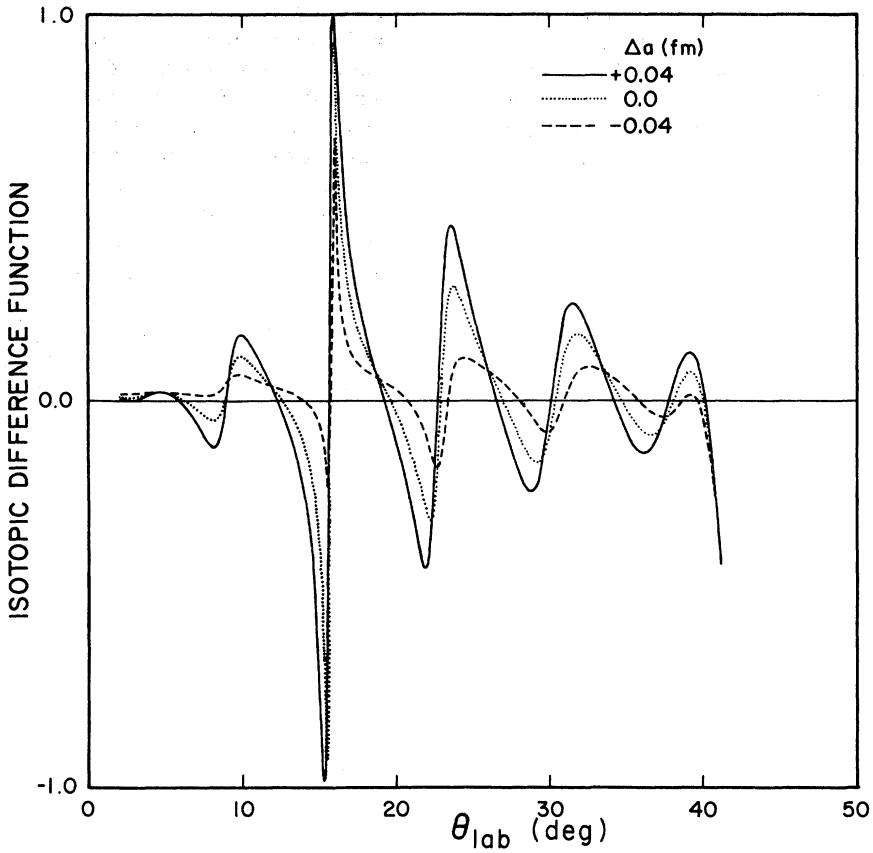


FIG. 6. Isotopic difference function for various values of $\Delta a = a(48) - a(40)$.

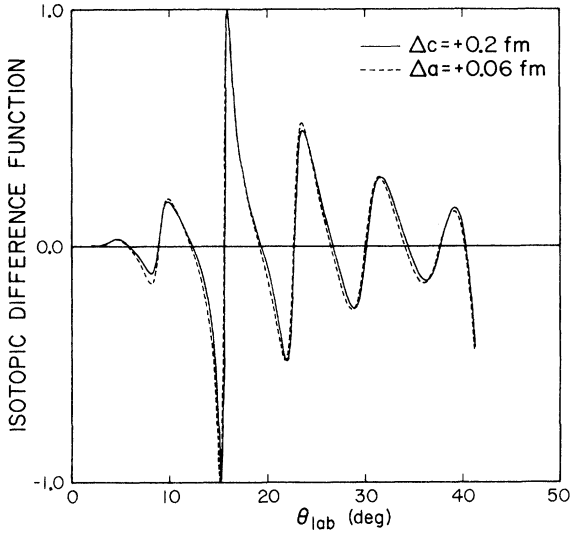


FIG. 7. Isotopic difference function for $\Delta R = 0.13$ fm. For the solid curve this is obtained by setting $\Delta c = 0.2$ fm and $\Delta a = 0$; for the dashed curve by setting $\Delta c = 0$ and $\Delta a = 0.6$ fm.

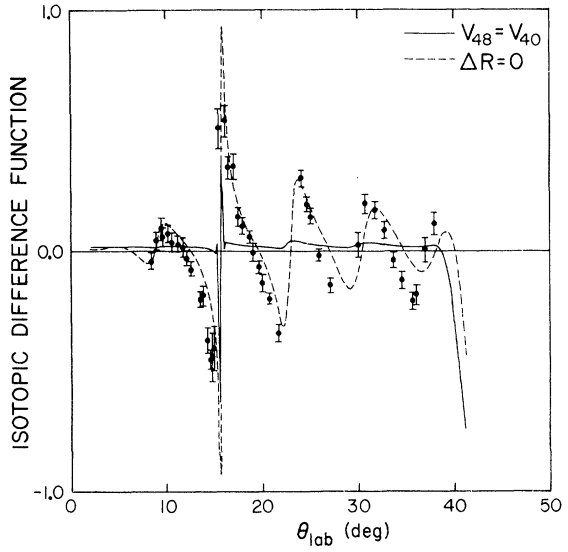


FIG. 8. Isotopic difference function. The solid curve shows the center of mass effect and is labeled by $V(48) = V(40)$, i.e., the optical potentials of $^{40,48}$Ca are the same. The dashed curve shows the normalization effect and corresponds to $\Delta R = 0$, i.e., $\rho_{48}(r) = (48/40)\rho_{40}(r)$.

where $\epsilon_i$ is the error in $D(\theta_i)$ and was taken to be the statistical error. As was previously shown $D(\theta)$ depends primarily on $\Delta R$ (the rms radius difference) and not $\Delta c$ or $\Delta a$ separately. The best fit occurs for $\Delta R = 0.02$ fm ($\chi^2 = 1.6$). Figure 9 shows the fits for $\Delta R = 0.06$ and $-0.02$ fm which correspond to $\chi^2/\chi^2_{\min} = 1.5$. In general it is found that for $\chi^2/\chi^2_{\min} = 1.5$ it is difficult to distinguish qualitatively the curves from the best fit ($\chi^2_{\min}$) so that a measure of the fitting error can be obtained when $\chi^2/\chi^2_{\min} = 1.5$. For the present case this gives $\Delta R = 0.02 \pm 0.04$ fm.

In general one can consider three sources of errors: (1) a fitting error discussed above (assuming only statistical errors); (2) systematic errors in the cross section of $^{48}$Ca relative to $^{40}$Ca and; (3) inaccuracies in the assumed model [Eqs. (1) and (2)]. The latter case will be discussed in Sec. III D. The first two types of error are indicated in Fig. 10. The fitting error is shown in Fig. 10(a) where $\chi^2$ is plotted versus $\Delta R$.

The uncertainty in $\Delta R$ caused by systematic errors in the cross section of $^{48}$Ca relative to $^{40}$Ca is shown in Fig. 10(b). The systematic error is estimated to be ~5% which corresponds to a range in $\Delta R$ from $-0.1$ to $+0.05$ fm and an uncertainty in $\Delta R$ of $\pm 0.03$ fm. This uncertainty is comparable to the $\pm 0.04$ fm fitting error.

Figure 11(a) compares the best fit value ($\chi^2 = 1.6$, $\Delta R = +0.02$ fm) with predictions based upon the Hartree-Fock calculations of Negele[12] ($\chi^2 = 12$, $\Delta R = 0.20$ fm) and of Miller-Green[13] ($\chi^2 = 4$, $\Delta R = 0.125$ fm). It is clear that the Negele calculation predicts too large an isotopic shift whereas the Miller-Green[13] calculation is in good agreement with the data (see Sec. IV). Figure 11(b) illustrates the effects of using surface absorption [Eq. (1b)] rather than volume absorption [Eq. (1a)]. The differences are negligible which indicates that the interior of $\mathrm{Im}U(r_\alpha)$ is not important (see Sec. III D). A complete analysis of the 79 MeV data was done with both surface and volume imaginary geometries. In no case were there statistically significant differences and either geometry may be used in what follows.

Figure 12 shows the analysis of the 41.8 MeV

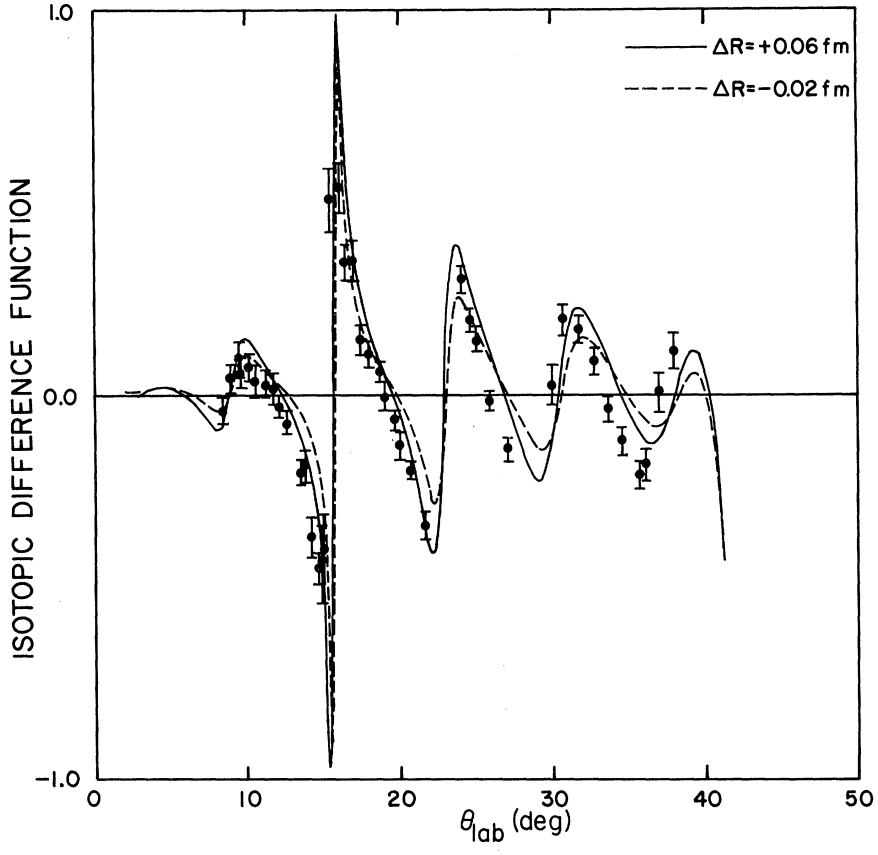


FIG. 9. Isotopic difference function. The two curves shown correspond to the error limits $\Delta R = 0.06$ and $-0.02$ fm of the best fit. The best fit corresponding to $\Delta R = 0.02$ fm is not shown.

data of Fernandez and Blair.[16] As noted in Ref. 11, the microscopic model is of marginal validity at this energy but the best fit result $\Delta R = 0.07$ fm with $\chi^2 = 3.9$ is in reasonable agreement with the higher energy data.

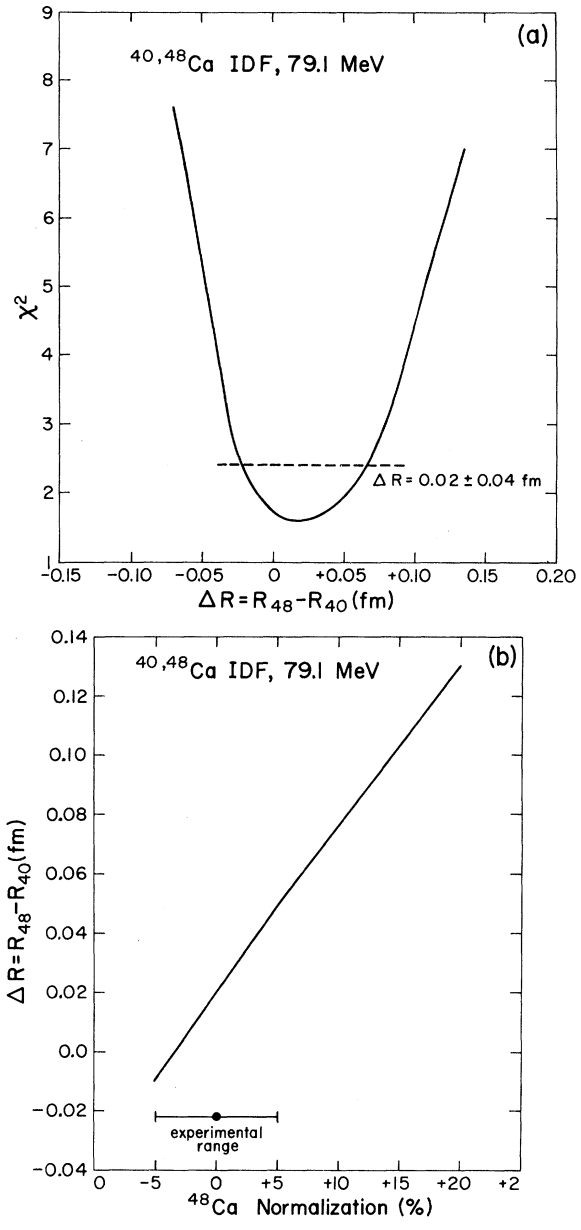


FIG. 10. (a) $\chi^2$ versus $\Delta R$ for the isotopic difference function. The minimum at $\Delta R = 0.02 \pm 0.04$ fm is indicated. The quoted error comes from the intercept with the line $\chi^2/\chi^2_{\min} = 1.5$ which is shown as a dashed line. (b) Best value of $\Delta R$ obtained as a function of the relative normalization of the experimental $^{48}$Ca cross sections relative to $^{40}$Ca. The experimental range of this variation (±5%) is indicated.

The values of $\Delta R$ obtained in this analysis are presented in Table I along with the average value $\Delta R = 0.05 \pm 0.04$ fm. The individual determinations are in good agreement with each other.

### C. $^{40,48}$Ca density and optical potential differences

In general it can be shown[6] that $\alpha$ particle scattering determines the density in the spatial region near $r = \bar{r}$ where $\rho(\bar{r}) \cong 0.017\ n/\text{fm}^3$ (about 10% of central density). For the optical potential $U(r_\alpha)$ there is also a spatial region near $r_\alpha = \bar{r}_\alpha \cong \bar{r} + 2.0$ fm for which $U(r_\alpha)$ is well determined.[6] In this section the determination of $\Delta\bar{r}$, $\Delta\rho(\bar{r})$, $\Delta\bar{r}_\alpha$, and $\Delta U(\bar{r}_\alpha)$ will be presented for $^{40,48}$Ca.

In fitting the isotopic difference function values

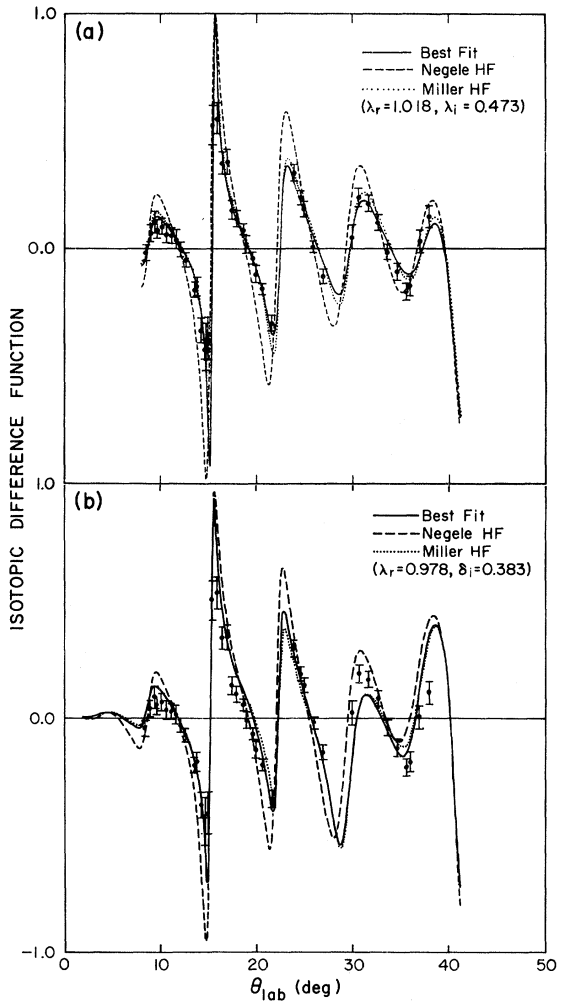


FIG. 11. Isotopic difference function. The best fit is compared to the Hartree-Fock predictions of Negele (Ref. 12) and Miller and Green (Ref. 13). Part (a) shows the calculation with volume absorption [Eq. (1a)] and part (b) with surface absorption [Eq. (1b)].

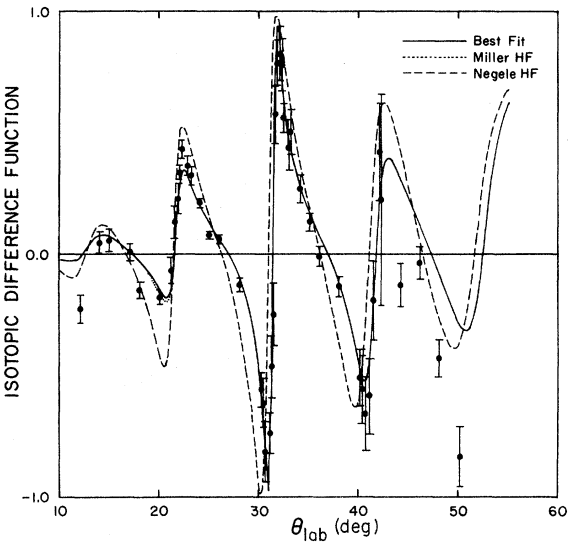


FIG. 12. Isotopic difference function at 42 MeV using the data of Ref. 16. The three curves are the best fit, the Hartree-Fock predictions of Negele (Ref. 12), and Miller and Green (Ref. 13). The Miller-Green prediction is essentially indistinguishable from the best fit curve.

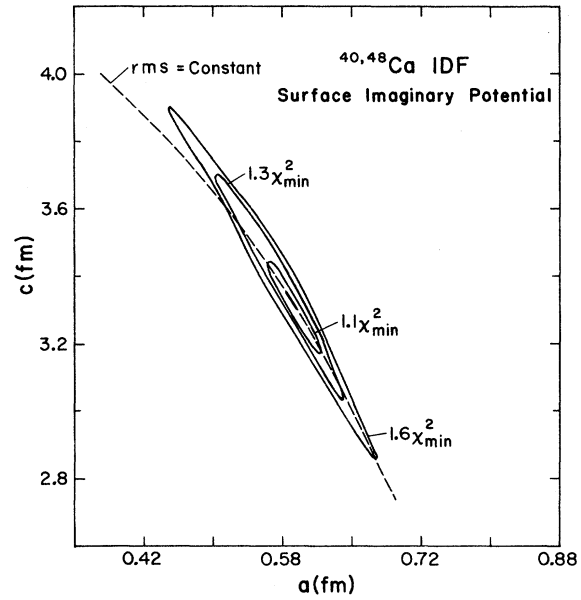


FIG. 13. Contours of constant $\chi^2$ found in fitting the isotopic difference function in the $c,a$ plane [where $c$ and $a$ are the parameters of $\rho(r)$ for $^{48}$Ca]. These curves were obtained by using the surface imaginary potential [Eq. (1b)]. They are very similar to the ones found using the volume imaginary potential [Eq. (1a)]. The curve for constant rms radius of $^{48}$Ca is also shown. For this calculation the density parameters of $^{40}$Ca were held constant.

of $c(48)$ and $a(48)$ in Eq. (3) are assumed. The contours of constant $\chi^2$ have been obtained and are presented in Fig. 13 (in the previous section the minimun value was discussed). These contours resemble elongated ellipses; the long axis is called the "soft direction." In Fig. 14(a) $r^2\Delta\rho$ is plotted for five $(c,a)$ values along the soft direction of the error ellipse. From this figure it is seen that all

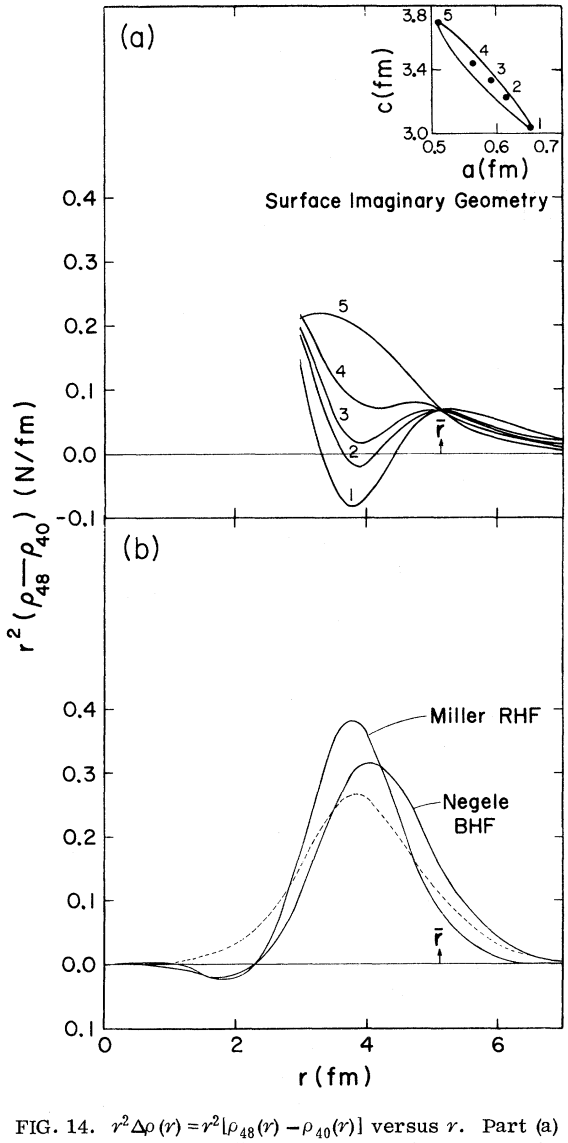


FIG. 14. $r^2\Delta\rho(r) = r^2[\rho_{48}(r) - \rho_{40}(r)]$ versus $r$. Part (a) is five points along the "soft direction" of the error ellipse of Fig. 13. The five points (labeled 1 through 5) are indicated in the insert. The crossover point at $r = \bar{r} = 5.1$ fm is indicated. The plot is shown for $r \gtrsim 3$ fm which is the region of sensitivity of $\alpha$ particle scattering. Part (1b) shows the theoretical Hartree-Fock predictions of Negele (Ref. 12) and Miller and Green (Ref. 13). The dashed curve is generated using Fermi densities with $c = 1.2A^{1/3}$ and $a = 0.57$ fm.

TABLE II. Results from the $D(\theta)$ analysis at 79.1 MeV for $\Delta\rho(\bar{r})$ and $\Delta U(\bar{r}_\alpha)$ for $^{40,48}$Ca. The critical radii are $\bar{r}=5.1$ fm [Fig. 14(a)] and $\bar{r}_\alpha=7.15$ fm [Fig. 15(a)]. The quoted uncertainties are obtained at the ends of the fitting error elipse having $\chi^2=1.3\chi^2_{\min}$.

| | Experiment | Negele HF | Miller HF |
|---|---|---|---|
| $\bar{r}^2\Delta\rho(\bar{r})$ (nucleons/fm) | 0.065±0.015 | 0.165 | 0.090 |
| $\Delta U(\bar{r}_\alpha)$ (MeV) | 0.83 ±0.07 | 1.80 | 0.95 |

of the $r^2\Delta\rho$ curves intersect at the point $r\equiv\bar{r}=5.1$ fm. Relative to the best fit curve (No. 3), if the other curves are larger for $r>\bar{r}$ they are smaller for $r<\bar{r}$ (or vice versa). This strong correlation is what insures that $\Delta R$ is well measured. This can be seen in Fig. 13 by the fact that the line for constant rms radius is very close to the "soft axis" of the ellipse.

Hartree-Fock predictions for $r^2\Delta\rho$ are presented in Fig. 14(b). The values at $r=\bar{r}$ are compared to the ones obtained from $\alpha$ particle scattering in Table II. It can be seen that the calculation of Miller and Green[13] is in reasonable agreement with experiment but that of Negele[12] is not. This will be discussed in Sec. V.

Corresponding to the point $\bar{r}$ for $\rho(r)$ there is a point $\bar{r}_\alpha$ for $U(r_\alpha)$. This point $\bar{r}_\alpha=7.15$ fm is determined by the location of the waist in the envelope of the curves in Fig. 15(a). As was anticipated, $\bar{r}_\alpha$ is approximately 2.0 fm larger than $\bar{r}$. The theoretical predictions for $\Delta U(r_\alpha)$ have been obtained by inserting the theoretical $\rho(r)$ values into Eq. (1) and are presented in Fig. 15(b) and in Table II. As is the case for $r^2\Delta\rho$, the calculations of Miller and Green[13] are in reasonable agreement with $\alpha$ particle scattering but those of Negele[12] are not.

### D. Estimate of model-dependent errors

As discussed in Sec. I, the strongly absorbing nature of the particle-nucleus interaction leads one to anticipate that the results of the present analysis should be insensitive to the details of the model assumed. In this section quantitative evidence is presented to support that hypothesis and an estimate of the model-induced error is made.

The first check concerns the form of the theoretically undefined imaginary part of $U(r_\alpha)$. As indicated in Fig. 1(a) the best fit to the scattering from $^{40}$Ca is essentially the same with surface or volume absorption. The best fits to the isotopic difference function [Eq. (5)] are shown in Fig. 11. Again there is essentially no difference in the quality of the best fit using either surface or vol-

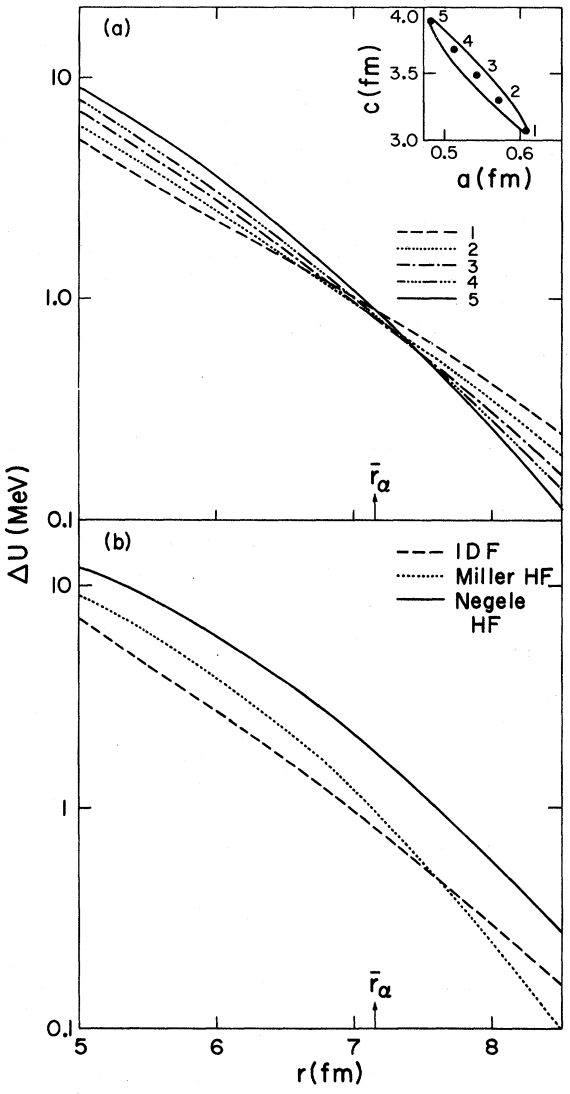


FIG. 15. Differences of the real part of the optical potential for $^{40,48}$Ca. Part (a) is for five points along the "soft direction" of the error ellipse of Fig. 13. The five points are labeled in the insert. The crossover point at $\bar{r}_\alpha=7.15$ fm is shown. Part (b) shows the best fit along with the Hartree-Fock predictions of Negele (Ref. 12) and Miller and Green (Ref. 13).

ume absorption and the value of $\Delta R = 0.02$ fm is the same in both cases. These results are presented in Table III and it is concluded that the results of $\alpha$ particle scattering in the diffraction region are largely insensitive to the form of the imaginary potential.

In order to check that the results do not depend critically on the values of the empirical parameters $\lambda_r$ and $\lambda_i$ they were varied by approximately 8% from their best values. With these values the scattering from $^{40}$Ca could not be even qualitatively reproduced. However a good fit to the isotopic difference function was achieved (since it is less sensitive to $\lambda_r$ and $\lambda_i$) with the result $\Delta R = 0.04$ fm, which is within the error of the best fit value (see Table III).

To check that the specific choice of $V_{\text{eff}}$ is not critical the analysis was repeated using a range $r_0$ [Eq. (2)] which was 10% smaller than the standard 2.0 fm case. The $\lambda$'s taken for this test were generated using the empirical relationship[23] $\lambda_{r,i} r_0^6 = \text{constant}$. A good fit to the isotopic difference function was obtained with a result of $\Delta R = 0.06$ fm which is within the error of the best fit value.

In order to check whether variations in the less understood imaginary part of Eq. (1) were causing a problem $\lambda_i$ was varied for $^{48}$Ca only. It was found that $\sigma(\theta)$ is fairly insensitive to $\lambda_i$ for $^{48}$Ca but that the best fit is obtained with the same value of $\lambda_i$ as for $^{40}$Ca. These results indicate that the difference in $\sigma(\theta)$ is dominated by the difference in $\rho(r)$ and the details of $V_{\text{eff}}$ are not important. The possible errors involved appear to be about the same as the fitting errors (~0.04 fm).

It should be emphasized that there is one critical assumption which is that $V_{\text{eff}}$ is the same in $^{40,41}$Ca. This requires that $\lambda_r$ (or $V_0$) and $r_0$ be the same for $^{40,48}$Ca. It may be instructive to inquire what changes in $\lambda_r$ or $r_0$ are required to obtain agreement with the HF calculations of Negele[12] who predicts $\Delta R = 0.20$ fm whereas the value found here is $\Delta R = 0.05 \pm 0.04$ fm.

It is possible to fit the $\alpha$ particle scattering from $^{40}$Ca with densities of different rms radii provided that compensating changes in the value of $\lambda_r$ are made.[11] For the values of $\lambda_r$ at $E_\alpha = 79$ MeV the relationship is $d\lambda_r/dR = -1.2$ fm$^{-1}$. If we take $dR = 0.15$ fm this gives $d\lambda_r = -0.18$ or $d\lambda_r/\lambda_r = -18\%$. This is a rather substantial change in $\lambda_r$ between $^{40,48}$Ca and seems quite unlikely.

The change can also be parametrized in terms of $r_0$, the range of $V_{\text{eff}}$ [Eq. (2)]. Suppose that $\lambda_r$ is the same in $^{40,48}$Ca but that $r_0$ changes. It has been previously shown[23] that changes in $r_0$ and $\lambda_r$ are equivalent to each other if

$$d\lambda_r/\lambda_r = 6 dr_0/r_0 .$$

For the present case $d\lambda_r/\lambda_r = -18\%$. One obtains $dr_0/r_0 = -3\%$. Since $r_0 = 2.0$ fm this makes $dr_0 = -0.06$ fm. These changes are based on changing $V_{\text{eff}}$ for *all* of the $^{48}$Ca nucleons. If one assumes that the interaction has been shown to be $A$-independent for the $N = Z$ core,[5] then the interaction can only differ for the eight valence nucleons in $^{48}$Ca. In order to obtain agreement with Negele's calculation,[12] the value of $dr_0$ for the valence nucleons would have to be six times larger than $dr_0$ for the core $dr_0 = r_0(\text{valence}) - r_0(\text{core}) \approx 0.36$ fm.

Although some $A$ dependence in either the strength or the range of the effective interaction cannot be arbitrarily ruled out, the required "relative" changes are quite large for two nuclei 8 amu apart. Previous analyses of $\alpha$ scattering from $^{16}$O, $^{28}$Si, $^{40}$Ca, $^{90}$Zr, and $^{208}$Pb found no evidence for an $A$-dependent interaction.

### E. $^{48}$Ca analysis

In the previous section $^{40,48}$Ca data were analyzed on a relative basis with the result that $\Delta R = 0.05 \pm 0.04$ fm. The rms radius of the charge distribution[22] of $^{40}$Ca is $R_c(40) = 3.452$ fm. Unfolding the proton size gives a proton rms radius $R_p(40) = 3.358$

TABLE III. Sensitivity of $\Delta R = R(48) - R(40)$ to changes in the $\alpha$ particle-nucleus interaction. The interaction is assumed to be the same in $^{40,48}$Ca.

| $r_0$ (fm) [a] | Interaction [b] | $\lambda_r$ | $\lambda_i(\delta_i)$ | $\chi^2$ | $\Delta R$ (fm) | Comments |
|---|---|---|---|---|---|---|
| 2.0 | Volume | 1.045 | 0.483 | 1.6 | $0.02 \pm 0.04$ | Best fit result |
| 2.0 | Surface | 0.978 | 0.383 | 2.6 | 0.01 | Check on the independence of the form of the imaginary potential |
| 2.0 | Volume | 0.96 | 0.52 | 3.6 | 0.04 | Arbitrary $\lambda_r, \lambda_i$ values |
| 1.8 | Volume | 1.87 | 0.86 | 2.0 | 0.06 | 10% change in the range of the interaction |

[a] The range of the effective $\alpha$ particle-nucleon interaction [Eq. (2)].
[b] Equation (1a) or (1b) used as indicated by volume or surface.

fm. Using the assumption that the rms matter radius $R(40) = R_p(40)$ with the measured $\Delta R$, one obtains $R(48) = 3.41 \pm 0.04$ fm. It is of interest to check this result using only the cross section data for $^{48}$Ca. In Fig. 16(a) the best fit on an absolute basis is presented from which one obtains $R(48) = 3.42 \pm 0.03$ fm in agreement with the value obtained from the isotopic difference function. In Fig. 16(b) the curve calculated using the density obtained from the isotopic difference function is presented and is also in good agreement with the data.

In Fig. 16 the HF predictions of Negele[12] and Miller and Green[13] are presented. It can be seen that the predictions of Miller and Green are in better agreement with the data than those of Negele. These are the same conclusions reached in the discussion of the isotopic difference function.

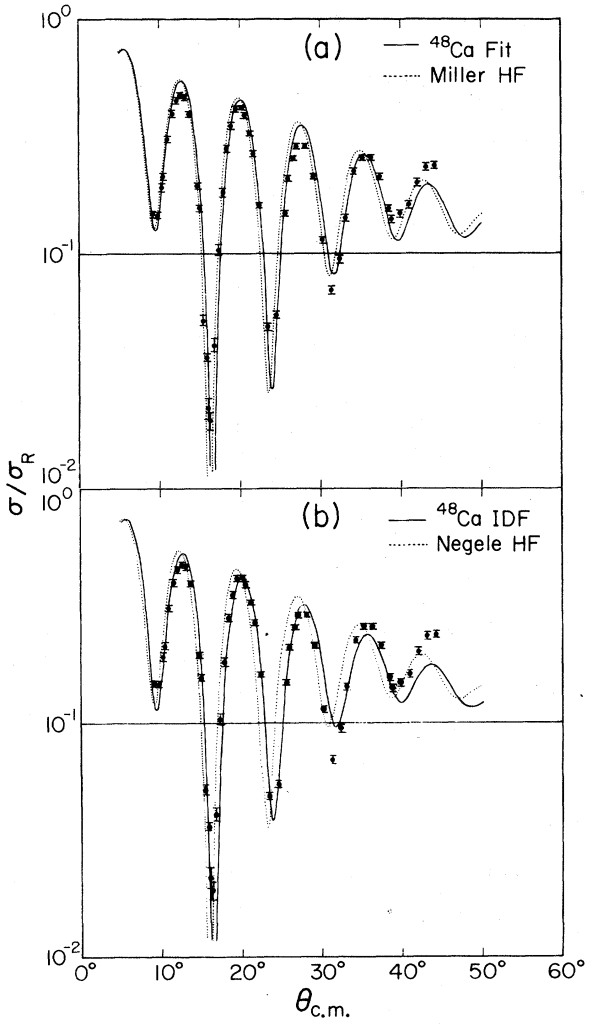


FIG. 16. Cross sections for $^{48}$Ca. Part (a) shows the best fit to the $^{48}$Ca data long with the Hartree-Fock predictions of Miller (Ref. 13). Part (b) shows the fit obtained with $\rho(r)$ determined using the isotopic difference function along with the Hartree-Fock prediction of Negele (Ref. 12).

### F. Neutron, proton differences in $^{48}$Ca

Combining the rms radii of the matter $R(48)$ and proton $R_p(48)$ distributions of $^{48}$Ca enable one to obtain the rms neutron radius $R_n(48)$ and thus to see if the neutrons extend beyond the protons. To do this we use the formula for the rms radius of a nucleus with $A = Z + N$:

$$R^2 = \frac{Z}{A} R_p^2 + \frac{N}{A} R_n^2 . \tag{7}$$

We define

$$\begin{aligned} &R_p(48) - R_p(40) \equiv \Delta_p = 0.01 \text{ fm} , \\ &R(48) - R(40) \equiv \Delta R , \\ &R_p(40) - R_n(40) \equiv 2\delta , \\ &R_n(48) - R_p(48) \equiv \delta_{np} , \end{aligned} \tag{8}$$

where $\Delta_p$ has been obtained[3] from electromagnetic experiments and $\Delta R$ is given in Table I. Substituting these definitions into Eq. (7) for $^{40}$Ca and $^{48}$Ca, and neglecting the squares of these differences, which are negligible, one obtains:

$$\delta_{np} = \tfrac{48}{28}(\Delta R - \delta - \Delta_p) . \tag{9}$$

One needs information about the unmeasured quantity $\delta$ in order to obtain $\delta_{np}$. Assuming $\delta = 0$ (neglecting Coulomb effects in $^{40}$Ca) and using the measured quantities results in $\delta_{np} = 0.07 \pm 0.07$ fm. Alternatively, $\delta$ can be obtained from Hartree-Fock calculations. This seems reasonable since $\delta$ originates from the Coulomb interaction and the Hartree-Fock calculations yield very accurate rms radii for $^{40}$Ca. In addition the values of $\delta$ from different Hartree-Fock calculations are in good agreement with each other (see Table V in Sec. V). We therefore assume a value of $\delta = 0.02$ fm from Hartree-Fock theory and obtain

$$\delta_{np} = 0.03 \pm 0.08 \text{ fm} .$$

This value is consistent with zero and is smaller than the Hartree-Fock predictions. It will be discussed further in Sec. V.

## IV. COMPARISON WITH OTHER EXPERIMENTS

The $^{40,48}$Ca sizes have been studied with the scattering of protons,[14,15] $\alpha$ particles,[7,16,17] and $^{16}$O ions.[18] The results of these measurements are presented in Table IV. Most earlier studies determined empirical optical potentials and charac-

TABLE IV. Summary of measurements of the $^{40,48}$Ca density and optical potential differences and of the $^{48}$Ca neutron-proton rms radii difference.

| Projectile (Method) | Projectile energy (MeV) | Reference | $\Delta R$ [a] (fm) | $\delta_{np}$ [b] (fm) | $\Delta R_V$ [c] (fm) | Definition of $R_V$ |
|---|---|---|---|---|---|---|
| $\alpha$ | 79 (42) [d] | This paper | 0.05 ± 0.04 | 0.03 ± 0.08 | 0.18 ± 0.04 | Diffraction radius |
| $\alpha$ | 166 | 7 | 0.21 ± 0.07 | 0.38 ± 0.12 | | |
| $\alpha$ | 42 | 16 | | | 0.11 to 0.24 | Various definitions of strong absorption (diffraction) radii |
| $\alpha$ | 31 | 17 | | | 0.15 | Radius parameter of Woods-Saxon potential |
| $^{16}$O | 20 to 40 | 18 | | | 0.41 ± 0.01 | Maximum of nuclear plus Coulomb potentials |
| $p$ | 10.8 to 16.3 | 14 | 0.22 ± 0.09 | 0.39 ± 0.10 | 0.24 ± 0.09 | rms radius of optical potential |
| $p$ | 25 to 40 | 15 | | | 0.15 | Radius parameter of Woods-Saxon potential |
| Coulomb energy difference | | 19 | | 0.06 | | |

[a] rms radius difference of $^{40,48}$Ca.
[b] Difference of neutron and proton rms radii in $^{48}$Ca.
[c] Difference of characteristic radii in $^{40,48}$Ca associated with the optical potential (see text).
[d] The 42 MeV data of Ref. 16 were also analyzed.

terize their results in terms of a radius parameter associated with the potential, denoted by $R_V$ in this paper. $R_V$ has been taken to be: the radius of a Woods-Saxon potential[15,17] with the assumption that the surface diffuseness $a$ is the same in $^{40,48}$Ca; the maximum of the nuclear plus Coulomb potential barriers[18]; the rms radius of the real part of the nuclear potential[14] (denoted by $R_V^*$ in this paper); the strong absorption or diffraction radii[16] which are determined from the phase shifts or from the real part of the optical potential (denoted by $R_D$ in this paper).

Several authors[15,17] have claimed on intuitive grounds that $\Delta R_V = \Delta R$ is equal to the rms radius difference between $^{40,48}$Ca. This is not true since $\Delta R_V$ is a model-dependent quantity whereas $R$ is not. Therefore it is important to present the results of this experiment in a way which can be

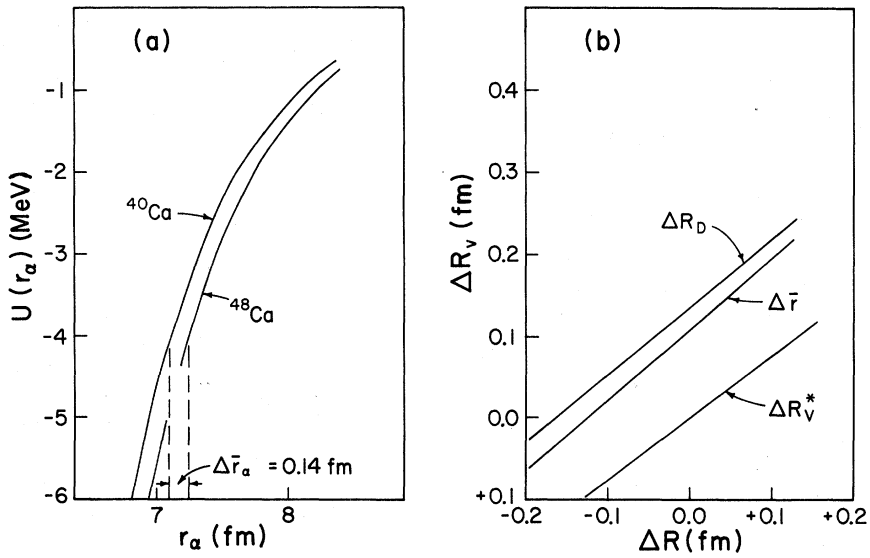


FIG. 17. Part (a) is the real part of the optical potential for $^{40,48}$Ca for the case of $\Delta R = 0$. This shows the normalization effect on the optical potential. The construction for $\Delta\bar{r}_\alpha = R_D$, the diffraction radius difference, is shown as the difference of these optical potentials at the value of −4.0 MeV. Part (b) shows $\Delta R_V$ versus $\Delta R$ where $\Delta R_V$ is taken to be $\Delta R_D$, $\Delta\bar{r}$, or $\Delta R_V^*$ (see text for discussion).

more readily compared with previous papers.

The real part of the optical potential for $\Delta R = 0$ is presented in Fig. 17(a). As discussed in Sec. III C, there is a point $\bar{r}_\alpha$ such that $\bar{r}_\alpha \cong \bar{r} + r_0$ (where $r_0$ is the range of $V_{\text{eff}}$). It is possible to identify $\bar{r}_\alpha$ with the diffraction radius $R_D$. For $^{40}$Ca $\bar{r}_\alpha \cong R_D = 7.1$ fm and $\text{Re}U(\bar{r}_\alpha) = -4.0$ MeV. One can therefore define $\Delta\bar{r}_\alpha = \Delta R_D$ for $^{40,48}$Ca to be the difference between the radii where the real part of the optical potentials equals $-4$ MeV. This construction is shown in Fig. 17(a) for the case $\Delta R = 0$ and it is seen that $\Delta\bar{r}_\alpha = \Delta R_D = 0.14$ fm.

One can calculate $\Delta\bar{r}$ and $\Delta\bar{r}_\alpha$ for various assumed values of $\Delta R$ and the results are presented in Fig. 17(b). The results of $\Delta R_V^*$, the difference in the rms radius of the potential, versus $\Delta R$ is also presented. The results are approximately straight lines with the most interesting point being that when $\Delta R = 0$ neither $\Delta\bar{r}$ or $\Delta\bar{r}_\alpha$ are zero although $\Delta R_V^* = 0$. For the best value $\Delta R = 0.05 \pm 0.04$ fm the corresponding value of $\Delta\bar{r}_\alpha = \Delta R_D$ is $0.18 \pm 0.04$ fm.

A comparison of the results in Table IV shows that the results of the present experiment are in agreement with those obtained with $\alpha$ particles at 42 [16] and 31 MeV [17] and in disagreement with the results of three experiments.[7,14,18] The agreement with the 42 MeV $\alpha$ particle results was previously shown in Sec. III (see Table I) by making the same analysis for that data as for the 79 MeV data obtained in the present experiment.

The results obtained with 166 MeV $\alpha$ particles[7] are the only other ones which have been analyzed with a microscopic analysis. Since these results are in disagreement with those found at three other $\alpha$ particle energies it is natural to assume that the problem is in the data and not in the analysis. It is likely that the problem is in the fact that the angular resolution was 0.7° in the 166 MeV experiment[7] and it can be seen from Figs. 2 and 4 that the angular differences are of that magnitude at 79 MeV and will be even smaller at 166 MeV. A more serious difficulty with the 166 MeV experiment is that the different targets were measured independently and not sequentially as in the present experiment. It is concluded that the 166 MeV experiment[7] was not accurate enough to measure the $^{40,48}$Ca difference correctly.

An experiment using $^{16}$O ions between 20 and 40 MeV,[18] which is in the Coulomb-nuclear interference region, has been performed. In this case the data were analyzed in terms of the radius $r_R$ at which the Coulomb plus nuclear potential has a maximum. The value of $\Delta r_R = 0.41$ fm which was obtained is very large. Although $r_R$ is an attractive quantity to obtain from such data, it is not clear how this radius is related to the density. Since $^{16}$O scattering is in a very preliminary stage it seems clear that more work has to be done on this subject.

Nuclear size information in $^{40,48}$Ca has been obtained from the elastic scattering cross sections and analyzing power measurements with polarized protons from 10.8 to 16.3 MeV.[14] The results were analyzed by use of an empirical Woods-Saxon optical potential with nine adjustable parameters. The rms radius of the real part of the potential was then related to the rms radii of the neutron and proton distributions. The results are presented in Table IV and can be seen to be significantly larger than those found in the present experiment. As can be seen from Fig. 17(b) one expects $\Delta R_V^* \cong \Delta R$ and the data in Table IV show that this is the case. Therefore the source of discrepancy between the proton results and this paper must be found from more fundamental reasons. We believe that there are four basic reasons for discounting the results of the proton experiment. First the energy of the experiment is low and the interpretation is really valid only at high energies.[24] For the case of $\alpha$ particle scattering it has been shown[11] that the microscopic approach is valid for bombarding energies $\gtrsim 50$ MeV. The proton scattering results from 25 to 40 MeV [15] are in agreement with the present experiment.

The second reason to suspect the results of Ref. 14 is that the experiment was not performed on the $^{40,48}$Ca targets sequentially. In fact, the experiments were not performed at the same energy for both targets and because of the low energies involved this could lead to large errors.

Third, there is the effect of the six empirical parameters of the imaginary and spin-orbit wells which were allowed to be different in $^{40,48}$Ca. No discussion of the effect of this type of parametrization is given. In particular no estimates of the error matrix between the spin-orbit and imaginary parts of the potential and the real part of the potential are presented. In view of this one can conclude that the stated errors are lower limits only and that all of the uncertainties of the model have been placed in the rms radii.

Fourth, there is the possibility that the rms radius of the potential is not uniquely determined by experiment. In a recent study of $^{16,17,18}$O with 65 MeV protons[24] it was found that different optical model fits to the $^{16}$O data differed in the rms radius of the real part of the optical potential by as much as 10%. (This paper[24] contains a general critique of the methods employed in deriving $R_n$ from proton scattering from another point of view.)

Finally, there is the lack of tests for the range of the effective interaction between the proton and the target neutrons and protons. In this respect

the advantage of the $\alpha$ particle as a projectile is clear because there is only one effective interaction (isoscalar) which can be found from the scattering from $T=0$ nuclei (e.g., $^{40}$Ca). For protons (or neutrons) as a projectile there are two effective interactions (isoscalar and isovector) and therefore in order to test the effective interaction one would have to scatter from an isoscalar nucleus and an isovector nucleus ($N>Z$) for which one knows both $\rho_p(r)$ and $\rho_n(r)$. It has been the practice to assume that the effective interaction is known and then to extract $R_n$ from the data.[24] It would seem that the range of the effective isovector interaction is not as well known as $R_n$ and that this procedure should be reversed.

It is concluded that $\alpha$ scattering is more reliable than nucleon scattering in determining $R$ and $R_n$ for two basic reasons. First, the interaction is isoscalar and can be determined with $T=0$ nuclei. Also, because $\alpha$ particles are strongly absorbed the elastic channel probes only the nuclear surface where it seems reasonable that the relation between the nuclear density and the optical potential [Eq. (1)] is independent of the specific target nucleus. A high degree of experimental precision is required, however, to extract these quantities from the data. In contrast to the other scattering results, the value of $\delta_{np}$ obtained from Coulomb energy differences[19] is in good agreement with the present result.

## V. COMPARISON WITH HARTREE-FOCK THEORY AND CONCLUSIONS

It is of interest to compare the results of this experiment with the predictions of Hartree-Fock (HF) theory.[12,13,25,26] These calculations have matured to the state where absolute rms charge radii are in excellent agreement with experiment. For example, the calculations of Negele[12] are in good agreement with electron scattering cross sections. The best experimental value for the rms proton radius of $^{40}$Ca (i.e., the charge radius with the proton size unfolded) taking into account the electron scattering[22] and muonic x-ray data[2] is $R_p = 3.38 \pm 0.02$ fm. The prediction of Negele[12] is $R_p = 3.40$ fm and that of Miller and Green[13] is $R_p = 3.37$ fm. The agreement is excellent, and it is not surprising that the density distributions of Negele and Miller and Green gave excellent agreement with the $\alpha$ particle scattering results for $^{40}$Ca (see Fig. 1).

In Table V a comparison of various rms radii differences are compared with experiment, whenever possible. The quantity $\delta = \frac{1}{2}[R_p(40) - R_n(40)]$ has not been measured and was used in our previous analysis (see Sec. III F). It is encouraging that for all of the quantities in the table there is good agreement between the different theoretical calculations.

The quantity $\delta_p = R_p(48) - R_p(40)$ has been the subject of several experimental investigations.[1,2] The lastest result,[3] taking the charge form factor of the neutron and certain relativistic effects into account is $+0.01$ fm.[3] Most of the HF calculations predict larger values, from 0.04 to 0.07 fm. The only dissenters are Miller and Green[13] who picked their parameters to obtain the previous result[1] of $-0.01$ fm which is really the difference of charge radii and not the difference of proton radii.[3]

The quantities of most direct concern to this experiment $\Delta R = R(48) - R(40)$ and $\delta_{np} = R_n(48) - R_p(48)$ are plotted in Fig. 18. It can be seen that

TABLE V. Comparison of Hartree-Fock predictions of rms radii of $^{40,48}$Ca with experiment.

| Reference | $\delta$ (fm) $\frac{1}{2}[R_p(40) - R_n(40)]$ | $\Delta R$ (fm) $R(48) - R(40)$ | $\Delta_p$ (fm) $R_p(48) - R_p(40)$ | $\delta_{np}$ (fm) $R_n(48) - R_p(48)$ | Notation in Fig. 18 |
|---|---|---|---|---|---|
| Negele (Ref. 12) | 0.021 | 0.190 | 0.042 | 0.227 | N |
| Miller and Green (Ref. 13) | 0.024 | 0.125 | −0.013 | 0.192 | M |
| Vautherin and Brink, Interaction I (Ref. 25) | 0.02 | 0.14 | 0.05 | 0.12 | $V_1$ |
| Vautherin and Brink, Interaction II (Ref. 25) | 0.025 | 0.17 | 0.05 | 0.18 | $V_2$ |
| Ehlers and Moszkowski (Ref. 26) | 0.03 | 0.21 | 0.07 | 0.19 | E |
| Average of Hartree-Fock Calc. | $0.024 \pm 0.004$ | $0.17 \pm 0.03$ | $0.04 \pm 0.03$ | $0.18 \pm 0.04$ | |
| Exp. | | $0.05 \pm 0.04$ [a] | 0.01 [b] | $0.03 \pm 0.08$ [a] | |

[a] This experiment.
[b] Reference 3.

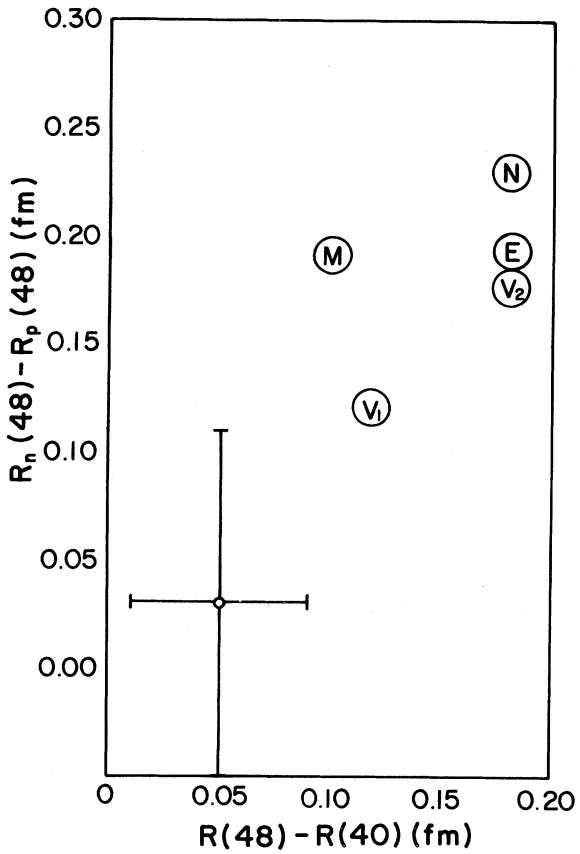


FIG. 18. $\delta_{np}=R_n(48)-R_p(48)$ versus $\Delta R$. The result of this experiment is shown with its error bar. The theoretical points are labeled as explained in Table V.

the value obtained for $\delta_{np}$ in this experiment is significantly smaller than those predicted by HF theory with the exception of the calculation of Vautherin and Brink interaction I.[25]

On the other hand, for $\Delta R$ this experiment is marginally in agreement with the predictions of Miller and Green[13] and Vautherin and Brink interaction I[25] for which $\Delta R \cong 0.1$ fm. The calculations of Negele,[12] Ehlers and Moszkowski,[26] Vautherin and Brink interaction II[25] for which $\Delta R \cong 0.2$ fm are not in agreement with this experiment. This has been shown in Figs. 11, 12, and 16 using the calculations of Miller and Green[13] and Negele[12] as representative of these two groups. From these figures it can be seen that any calculation which predicts $\Delta R \cong 0.2$ fm is in significant disagreement with this experiment, if the sensitivity of the method is reasonably represented by the quoted errors in the experiment. The fact that the prediction of Miller and Green[13] is in better agreement with the present results does not necessarily mean that theirs is the superior calculation. Indeed, for purely theoretical reasons the calculations of Negele[12] are on a firmer foundation, and also are in better agreement with electron scattering data.

The average of the five HF results was computed and presented in Table V. The quoted errors are the rms deviations from the mean which are gratifyingly small. This average is in disagreement with the results of this experiment for both $\Delta R$ and $\delta_{np}$.

The discrepancy between the results of this experiment and HF theory is hard to understand. As was stated earlier, the HF theory gives good predictions[12] for electron scattering for nuclei from $^{16}$O to $^{208}$Pb and it is difficult to believe that the proton distributions could be properly predicted while the neutron distributions were in error. Furthermore it has been shown that the HF calculations of Negele predict density distributions which are in excellent agreement with $\alpha$ particle scattering for $^{16}$O, $^{40}$Ca, $^{90}$Zr, and $^{208}$Pb for particle energies of 79 and 104 MeV[6] (the two energies for which data on a number of elements are available). This tests the neutron distribution as predicted by Negele. Alternatively, if one chooses to believe the HF calculations because they agree with electron scattering, then this can be thought of as checking the $\alpha$ scattering theory presented here.

In light of these arguments why should there be a discrepancy for $^{48}$Ca and not $^{16}$O, $^{40}$Ca, $^{90}$Zr, or $^{208}$Pb? The data have been carefully checked. One notes that the 79, 42, and 31 MeV data are in agreement (they were obtained in three different laboratories). It is true that the HF theory does not conserve isospin and neglects configuration mixing and it could be that one of these effects is particularly significant in $^{48}$Ca. Possibly some of the simplifications made in the $\alpha$ particle scattering analysis (e.g., neglect of exchange) are particularly significant in obtaining the small $^{40,48}$Ca differences.

It is a pleasure to acknowledge fruitful discussions with many of our colleagues, particularly John Schiffer, John Negele, and J. Heisenberg.

*Present address: Computer Sciences Corporation, Silver Spring, Maryland 20910.
†Present address: Department of Chemistry, Washington University, St. Louis, Missouri 63130.
‡Work supported in part by the National Science Foundation.
§Work supported in part by the U. S. Atomic Energy Commission Contract No. AT-(30-1)-2098.

[1]R. F. Frosch *et al.*, Phys. Rev. 174, 1380 (1968).
[2]R. D. Ehrlich *et al.*, Phys. Rev. Lett. 18, 959 (1967).
[3]W. Bertozzi, J. Friar, J. Heisenberg, and J. W. Negele, Phys. Lett. 41B, 408 (1972).
[4]D. F. Jackson, Phys. Lett. 32B, 233 (1970); C. G. Morgan and D. F. Jackson, Phys. Rev. 188, 1758 (1969); D. F. Jackson and V. K. Kembhavi, *ibid.* 178, 1626 (1969).
[5]A. M. Bernstein and W. A. Seidler, II, Phys. Lett. 34B, 569 (1971).
[6]A. M. Bernstein and W. A. Seidler, II, Phys. Lett. 39B, 583 (1972); (unpublished).
[7]B. Tatischeff, I. Brissaud, and L. Bimbot, Phys. Rev. C 5, 234 (1972); I. Brissaud *et al.*, Nucl. Phys. A191, 145 (1972).
[8]A. M. Bernstein, *Advances in Nuclear Physics* (Plenum, New York, 1969), Vol. III, p. 325.
[9]P. Mailandt, J. S. Lilley, and G. W. Greenlees, Phys. Rev. Lett. 28, 1075 (1972).
[10]I. Riechstein and Y. C. Tang, Nucl. Phys. A139, 144 (1969).
[11]G. M. Lerner, J. C. Hiebert, L. L. Rutledge, Jr., and A. M. Bernstein, Phys. Rev. C 6, 1254 (1972).
[12]J. W. Negele, Phys. Rev. C 1, 1260 (1970).
[13]L. D. Miller and A. E. S. Green, Phys. Rev. C 5, 241 (1972); L. D. Miller (private communication).
[14]J. C. Lombardi, R. N. Boyd, R. Arking, and A. B. Robbins, Nucl. Phys. A188, 103 (1972).
[15]C. J. Maggiore, C. R. Gruhn, T. Y. T. Kuo, and B. M. Preedom, Phys. Lett. 33B, 571 (1970).
[16]B. Fernandez and J. S. Blair, Phys. Rev. C 1, 523 (1970).
[17]A. M. Bernstein, M. Duffy, and E. P. Lippincott, Phys. Lett. 30B, 20 (1969).
[18]M. C. Bertin, S. L. Tabor, B. A. Watson, Y. Eisen, and G. Goldring, Nucl. Phys. A167, 216 (1971).
[19]J. A. Nolen, Jr., and J. P. Schiffer, Annu. Rev. Nucl. Sci. 19, 1560 (1969).
[20]See Ref. 6 for a brief review of the literature.
[21]J. S. Blair, *Lectures in Theoretical Physics* edited by P. D. Kunz, D. A. Lind, and W. E. Brittin (Univ. of Colorado Press, Boulder, 1966), Vol. VIIIC.
[22]J. Heisenberg (private communication).
[23]C. J. Batty, E. Friedman, and D. F. Jackson, Nucl. Phys. A175, 1 (1971).
[24]G. M. Lerner, Nucl. Phys. A205, 385 (1972).
[25]D. Vautherin and D. M. Brink, Phys. Rev. C 5, 626 (1972).
[26]J. W. Ehlers and S. A. Moszkowski, Phys. Rev. C 6, 217 (1972).